State-dependent modulation of activity in distinct layer 6 corticothalamic neurons in barrel cortex of awake mice

Suryadeep Dash,[1] Dawn M. Autio,[1] and Shane R. Crandall[1,2]

[1]Department of Physiology
Michigan State University
East Lansing, MI 48824

Phone: 517-884-5055

[2]Lead Contact

Correspondence: cranda86@msu.edu and suryadeep.dash@gmail.com

ABSTRACT

Layer 6 corticothalamic (L6 CT) neurons are in a strategic position to control sensory input to the neocortex, yet we understand very little about their functions. Apart from studying their anatomical, physiological and synaptic properties, most recent efforts have focused on the activity-dependent influences CT cells can exert on thalamic and cortical neurons through causal optogenetic manipulations. However, few studies have attempted to study them during behavior. In an attempt to address this gap, we performed juxtacellular recordings from optogenetically identified CT neurons in whisker-related primary somatosensory cortex (wS1) of awake, head-fixed mice (of either sex) free to rest quietly or self-initiate bouts of whisking and locomotion. We found a rich diversity of response profiles exhibited by CT cells. Broadly, their spiking patterns were either modulated by whisker-related behavior (~28%) or not (~72%). Whisker-related neurons exhibited both increases as well as decreases in firing rates. We also encountered cells with preceding modulations in firing rate before whisking onset. Overall, whisking better explained these changes in rates than overall changes in arousal. The CT cells that showed no whisker-related activity had low spontaneous firing rates (<0.5 Hz), with many all but silent. Remarkably, this relatively silent population preferentially spiked at the state transition point when pupil diameter constricted and the mouse entered quiet wakefulness. Thus, our results demonstrate that L6 CT neurons in wS1 show diverse spiking patterns, perhaps subserving distinct functional roles related to precisely timed responses during complex behaviors and transitions between discrete waking states.

INTRODUCTION

Layer 6 corticothalamic (L6 CT) neurons give rise to a massive descending projection that terminates in the thalamus. In core sensory systems, these fibers outnumber ascending thalamocortical axons by 10:1, and CT axons contribute far more synapses than peripheral afferents (Sherman and Koch, 1986; Liu et al., 1995; Erisir et al., 1997; Deschenes et al., 1998; Van Horn et al., 2000; Winer et al., 2001). In addition, L6 CT cells send local axon collaterals to the more superficial layers of the cortex that receive thalamic input (Gilbert and Wiesel, 1979; White and Keller, 1987; Zhang and Deschenes, 1997; Kim et al., 2014). Consequently, L6 CT neurons are strategically able to influence thalamic throughput and sensory responsiveness in the cortex.

Despite the anatomical prominence and a great deal of experimental effort focused on it (for review, see (Cudeiro and Sillito, 2006; Briggs and Usrey, 2008; Briggs, 2020), a thorough understanding of CT functions remains elusive. This lack of clarity is partly due to the technical challenges of monitoring or selectively manipulating CT activity. However, recent advances in optogenetic tools and the transgenic mouse line *Ntsr1-Cre* (Gong et al., 2007), which expresses Cre recombinase in L6 CT cells, have helped overcome these limitations, accelerating inquiry into the functional roles of the CT pathway.

One key feature to emerge from these studies is that the net effect (suppressive or enhancing) generated by L6 CT cells is likely to depend on the timing and rate at which they fire, with the sign and magnitude depending on their interactions with different excitatory and inhibitory circuit components (Olsen et al., 2012; Bortone et al., 2014; Mease et al., 2014; Crandall et al., 2015; Kim et al., 2015; Guo et al., 2017; Hasse and Briggs, 2017; Kirchgessner et al., 2020). However, a potential concern in using opsins to

manipulate CT activity is that the uniform activation or suppression generated within the pathway may differ considerably from naturally evoked patterns and thus affect thalamic and cortical activity differently. Furthermore, this approach ignores CT subtypes with perhaps different *in vivo* activity profiles and functional roles (Tsumoto and Suda, 1980; Landry and Dykes, 1985; Sirota et al., 2005; Briggs and Usrey, 2009; Kwegyir-Afful and Simons, 2009). Thus, an open and unresolved question is whether L6 CT neurons show variations in their firing rates consistent with those necessary to modulate downstream targets and if their behavior varies across cells. This question is of particular interest, given most studies across modalities and species report that CT cells *in vivo* are silent and lack suprathreshold responses to sensory input in both anesthetized and awake animals (Tsumoto and Suda, 1980; Swadlow and Weyand, 1987; Swadlow and Hicks, 1996; Sirota et al., 2005; Kwegyir-Afful and Simons, 2009). In addition, because CT regulation is dynamic, state-dependent, and likely context-dependent (Steriade, 2001; Lee et al., 2008; Velez-Fort et al., 2018), it is critical to investigate the CT system in awake, behaving subjects, something only a few studies have attempted (Beloozerova et al., 2003; Sirota et al., 2005; Augustinaite and Kuhn, 2020a; Voigts et al., 2020; Clayton et al., 2021).

To determine the activity patterns in the CT pathway of actively behaving animals, we used single-cell juxtacellular recordings to study the spiking properties of optogenetically identified CT neurons in the whisker-related primary somatosensory cortex (wS1) of awake, head-fixed mice free to rest quietly or self-initiate bouts of whisking and locomotion. Rodents actively move their whiskers forward and backward to gather spatial and textual information from their nearby environment, and the activity patterns in

wS1 contribute to tactile perception and sensorimotor processing (Diamond et al., 2008; Petersen, 2019). Yet no study has systematically recorded and functionally characterized the activity of identified L6 CT neurons in wS1 during exploratory whisking and locomotion behavior. We report diverse response types and significant spike rate modulation in L6 CT neurons during active whisking behavior and transitions between discrete waking states.

RESULTS

Optogenetic tagging and functional identification of L6 CT neurons in wS1

To investigate the behavior of L6 CT cells in awake, behaving mice, we used an *in vivo* Channelrhodopsin (ChR2)-assisted patching strategy to target individual genetically identified CT neurons for juxtacellular recording (Lima et al., 2009; Moore and Wehr, 2013; Munoz et al., 2014; Munoz et al., 2017; Yu et al., 2019). For these experiments, we took advantage of the *Ntsr1-Cre* driver mouse line (Gong et al., 2007), which selectively labels L6 CT neurons in sensory cortices, including wS1 (Bortone et al., 2014; Kim et al., 2014; Crandall et al., 2015; Guo et al., 2017). Consistent with previous reports, we found that *Ntsr1-Cre* positive somata in wS1 were restricted to L6 and that their axons/terminals were present in whisker-related nuclei of the somatosensory thalamus (**Fig. 1*A***). To render genetically defined CT neurons responsive to light, we conditionally expressed the light-sensitive cation channel ChR2 by either crossing the *Ntsr1-Cre* driver mouse to a reporter mouse line (Ai32) that conditionally expresses ChR2-enhanced yellow fluorescent protein (ChR2-EYFP) or by viral transduction with a Cre-dependent adeno-associated virus expression vector (AAV) (Madisen et al., 2012; Crandall et al., 2015). To directly relate CT activity to behavior and waking state, we recorded individual cells located across the depth of L6 in awake, head-fixed mice positioned on a flexible wheel-apparatus while simultaneously monitoring the mystacial-pad EMG for whisking, pupil diameter for changes in general arousal, and wheel movement for locomotor bouts (**Fig. 1*B*, left**). Previous studies have shown pupil diameter to be a reliable index of arousal state in mice (Reimer et al., 2014; McGinley et al., 2015a; Vinck et al., 2015). For identification of L6 CT cells *in vivo*, we used a brief focal LED stimuli (465 nm, 5 ms, 2

Hz, 3-8 mW) directed through the glass recording pipette to stimulate ChR2-expressing CT cells effectively at the tip of the pipette (**Fig. 1*B*, right**).

Figure 1C shows an example of a photo-activated neuron identified as a CT cell based on the characteristics of its light-evoked activity. This neuron had a cumulative spike probability of one within the first 3 ms of LED onset. Following the recording, we labeled the cell with neurobiotin by juxtacellular iontophoresis and confirmed ChR2 expression histologically (Pinault, 1996) (**Fig. 1*D***). We observed similar light-evoked activity in 6 cells confirmed posthoc as expressing ChR2. Consistent with this observation, we found that histologically recovered cells with a low spike probability (< 0.5) or a significant delay to light-evoked responses (> 5 ms) were negative for ChR2 expression (8 cells, data not shown). Across the entire population, identified L6 CT cells had a spike probability of 0.5 or greater and a cumulative probability of 1.0 or greater within 3 ms and 5 ms of LED onset, respectively (n = 115 cells from 27 mice; 17 males and 10 females) (**Fig. 4*E***). Thus, high spike probability and short-latency to peak spike probability are reliable physiological criteria for identifying ChR2-expressing L6 CT neurons *in vivo*.

Since CT activity recruits fast-spiking (FS) inhibitory interneurons (Beierlein and Connors, 2002; Bortone et al., 2014; Frandolig et al., 2019), we performed additional analyses on spike waveform components to separate putative FS neurons from our CT population. We found that a small number of neurons met our light-evoked criteria (n = 22 cells), but these neurons displayed electrophysiological signatures of putative FS cells (Simons, 1978; Bortone et al., 2014; Yu et al., 2019), with their recorded spikes having a peak-to-trough time less than 0.5 ms (0.28 ± 0.05 ms; as compared with CT cells 0.62 ±

0.16 ms), and a lower peak-trough ratio (1.73 ± 0.55; as compared with CT cells 3.76 ± 1.39) (**Fig.1*F***). Putative FS cells also had a longer latency to peak spike probability (4.31 ± 0.65 ms) from LED onset than CT neurons (2.85 ± 1.16 ms; **Fig.1*F***, right). Therefore, our dataset likely represents exclusively excitatory L6 CT cells.

Three broad classes of L6 CT cells based on their activity patterns in awake mice

We recorded the activity of all L6 CT neurons encountered by our pipette (n = 115) during simple free behavior, in which the head-fixed mouse was allowed to rest quietly or self-initiate whisker-related behavior. Based on the measured EMG signal and recorded wheel movement, we defined the behavioral state of the mice as 1) quiet wakefulness with no whisker movement, 2) whisking, and 3) whisking with concomitant locomotion (whisking/locomotion). Consistent with previous observations (Sofroniew et al., 2014; Ayaz et al., 2019), mice never walked/ran on the wheel without whisking.

We found that the activity patterns differed considerably among CT neurons, even within a single electrode penetration (**Fig. 2**). Consistent with several previous studies in other species and sensory cortices (Tsumoto and Suda, 1980; Swadlow, 1994; Beloozerova et al., 2003; Sirota et al., 2005; Stoelzel et al., 2017), we found that most L6 CT cells in wS1 of mice were virtually silent, displaying low spontaneous firing rates and no evoked activity during whisking or locomotion (Silent-type: 72%; 83 of 115 CT neurons; **Fig. 2*A***). Furthermore, although the majority of silent-type CT cells (60.2%; 50 of 83 silent-type neurons) had a firing rate of less than 0.5 spikes/s (mean: 0.22 ± 0.55 spikes/s), several cells never fired spontaneously during the entire recording session (completely silent: 39.8%; 33 of 83 silent-type neurons).

The remaining L6 CT cells showed robust modulation in firing rates during whisking or whisking/locomotion (28%; 32 of 115 CT neurons; **Fig. 2*B and C***). Approximately 60% (19 of 32) of the modulated L6 CT cells had negligible firing rates during quiet wakefulness but were active during whisking episodes, increasing their firing rates around either solitary whisking or bouts of whisking/locomotion or both (Active-type: **Fig. 2*B***). Conversely, roughly 40% (13 of 32) of the modulated CT cells were spontaneously active during quiet wakefulness but reduced spiking activity during whisking and whisking/locomotion (Pausing-type: **Fig. 2*C***). Therefore, most L6 CT neurons in wS1 of awake mice are relatively silent, whereas approximately one-third of the cells showed distinct whisker-related modulations in firing rate.

Diverse response types of L6 CT cells during whisker-related behaviors

Further examination of the non-silent CT population revealed important relationships between whisker-related behavior and neuronal firing rate. Specifically, we found that the active-type CT cells showed diverse responses and significant modulation of spiking rates during whisking/locomotion that comprised tonic increases in spike rate, phasic increases in the rate at whisking onset, elevated firing rates before whisking onset, and delayed activity (**Fig. 3*A***, Active-type, from left to right). In addition, most active-type CT cells (68%; 13 of 19) increased spiking during solitary whisking, with the only exception being those that had delayed activity with locomotion (**Fig. 3*B***), suggesting changes in firing rates are not only associated with locomotion. In contrast, pausing-type CT cells exhibited less diverse responses, with most responding with a decrease in spike rate during whisking/locomotion and whisking (**Fig. 3*A, B***). However, we did encounter three

pausing-type CT cells with more complex firing patterns, such as responding bimodally, with first a decrease and then an increase in firing rate during locomotion. **Figure 3*C*** shows the qualitative summary of the spiking profiles of all CT cells modulated during whisking/locomotion and whisking.

We next quantified the cell-type-specific modulation of firing rates during whisker-related behaviors. On average, the mean firing rates of the active-type CT cells (n = 19) were low during baseline periods of quiet wakefulness before whisker-related behaviors (before whisking: 1.5 ± 1.7 spikes/s; before whisking/locomotion: 1.9 ± 2.6 spikes/s). During bouts of solitary whisking, the mean discharge rates of active-type CT cells were significantly higher than baseline (3.04 ± 3.23 spikes/s; p = 5.16e-04; Wilcoxon paired signed-rank test; **Fig. 3*D***, top blue circles). Responses were also significantly elevated during whisking/locomotion, becoming more intense, with some active-type CT cells having high firing rates (10.12 ±12.2 spikes/s; p = 8.85e-05; Wilcoxon paired signed-rank test; **Fig. 3*D***, top red circles). The peak firing rates across all active-type CT cells sampled were significantly higher during whisking/locomotion (22.87 ± 21.16 spikes/s) than whisking (6.5 ± 6.7 spikes/s) (p = 1.033e-04; Wilcoxon paired signed-rank test, **Fig. 3*D***, bottom). Some active-type CT cells (32%; 6 of 19) exhibited elevated spike rates during whisking/locomotion but not whisking, and therefore we classified these cells as locomotion-related and excluded them from subsequent analyses.

All pausing-type CT cells (n = 13) were spontaneously active during the period of quiet wakefulness preceding whisker-related behaviors (before whisking: 6.3 ± 5.2 spikes/s; before whisking/locomotion: 7.3 ± 5.6 spikes/s). However, the mean firing rate of these neurons significantly decreased during whisking (5.0 ± 4.0 spikes/s; p = 1.03e-

04; Wilcoxon paired signed-rank test; **Fig. 3*E***, top blue circles) and whisking/locomotion (2.6 ± 4.8 spikes/s; p = 0.03; Wilcoxon paired signed-rank test; **Fig. 3*E***, top red circles). The three pausing-type CT cells with a mean firing rate higher during whisking/locomotion (red data points above the diagonal) correspond to those that responded bimodally, with an initial decrease followed by an increase in spiking activity during locomotion epochs. Across all pausing-type CT cells recorded, the lowest level (trough) of instantaneous spike rate during whisking/locomotion (0.6 ± 1.1 spikes/s) was lower than that observed for whisking (2.7 ± 2.4 spikes/s; p = 2.44e-04; Wilcoxon paired signed-rank test; **Fig. 3*E***, bottom).

In summary, approximately one-third of the L6 CT cells recorded in wS1 of awake, head-fixed mice exhibited robust whisker-related modulation of firing rates, with individual CT neurons characterized by increases (active-type) or decreases in discharge rates (pausing-type). In addition, all neurons exhibited greater firing rate modulation during whisking/locomotion than bouts of whisking only.

Pre-movement modulation of firing rate in some L6 CT cells of wS1

For many non-silent L6 CT neurons, we often observed changes in spiking rates that preceded whisker-related behavior, as measured by the electrical activity generated in the muscles of the mystacial pad (i.e., EMG signal). To assess the temporal relationship between whisker movement and a change in neural activity, we characterized the firing rate changes in whisker-related L6 CT neurons (active- and pausing-type) as a function of time around the onset of self-initiated whisking. We defined a change in instantaneous spiking activity as a 30% deviation (above or below) from the average pre-whisking

baseline activity (2 s). This criterion was conservative and biased towards delaying onset detection. Since the analysis depended on baseline activity, we selected only neurons with stable rates above 2.0 spikes/s. Among all the active- and pausing-type CT cells recorded, 38% (5 of 13) and 77% (10 of 13) met this criterion for analysis, respectively.

Figure 4*A* shows two active- and pausing-type L6 CT neurons with a firing rate change (black dotted line) detected before EMG onset (red dotted line), respectively. Of the five active-type CT cells analyzed, 80% (4 of 5 cells) exhibited rate changes that increased before whisker movement (mean: -118 ± 178 ms, n = 5 cells, **Fig. 4*B***, top). Similarly, the discharge rate in 90% (9 of 10 cells) of pausing-type CT cells decreased before EMG onset (mean: -248 ± 206 ms, n = 10 cells, **Fig. 4*B***, bottom). Since we performed the above analysis on whisking/locomotion, we repeated the analysis on bouts of solitary whisking. Due to the variability in EMG signal related to whisking, we focused our analysis on the strongest 50% of all whisks identified for each cell based on the peak EMG signal. We found that most active- and pausing-type CT cells showed similar spiking rate changes before solitary whisking. Altogether, these data suggest that a subset of L6 CT cells in wS1 change their firing rate well before self-initiated whisker movements, with and without subsequent locomotion.

The transition from quite awake to exploratory behaviors such as whisking and locomotion is associated with changes in arousal (McGinley et al., 2015b). To help understand the contributions of arousal to the observed changes in L6 CT firing rates, we analyzed changes in pupil diameter, which is a reliable index for general arousal in head-fixed mice (Reimer et al., 2014; McGinley et al., 2015a; Vinck et al., 2015). Consistent with these previous studies, we observed that the onset of locomotion is preceded by an

increase in pupil diameter, which ramped up hundreds of milliseconds before, suggesting that general arousal may contribute to the pre-movement modulation of CT activity (n = 32 behavioral sessions obtained from the 32 whisker-related CT cells; **Fig. 4D**). However, while pupil diameter increased 500-1000 ms before EMG onset during whisking/locomotion, we found that during solitary whisking, the increases in the EMG signal preceded increases in pupil diameter by 250-500 ms (**Fig. 4E-F**). These results suggest that the pre-movement modulation of L6 CT circuit activity may also represent a motor-preparatory signal.

To assess the contributions of arousal and motor activity to the cell-type-specific modulation of spiking rate observed in whisker-related L6 CT cells, we calculated the cross-correlation coefficient between EMG signal or pupil diameter and the instantaneous spiking rate around whisking onset. Analysis of the time courses of EMG signals and pupil dynamics revealed a moderately strong correlation and anti-correlation with spiking activity for most active- and pausing-type CT cells, respectively, during both whisking/locomotion and whisking (**Fig. 5A-B**). Overall, we found that the best absolute cross-correlation (irrespective of lags or leads) for both active- and pausing-type cells was consistently stronger with EMG than with pupil during whisking/locomotion and whisking (**Fig. 5C-D**, left). Moreover, we found that EMG signals generally aligned with the spiking activity of whisker-related CT cells with a much shorter lag compared to pupil dynamics (**Fig. 5C-D**, right). Altogether, these results indicate a stronger correlation and better temporal alignment between the firing rates of whisker-related CT cells and the time course of the EMG (motor) signal than pupil (arousal) dynamics.

Relationship between pupil diameter and spiking activity of silent CT cells

Like S1 CT cells in other species (Landry and Dykes, 1985; Swadlow, 1989, 1990; Swadlow and Hicks, 1996; Kelly et al., 2001; Lee et al., 2008; Kwegyir-Afful and Simons, 2009), most L6 CT cells recorded in the present study showed very little spontaneous activity or whisker-related responses (72%; **Fig. 2*A***). The function of these silent cells is enigmatic. Here, we routinely observed that some silent-type CT cells with low spontaneous firing exhibited a strong relationship to the moment-to-moment fluctuations in pupil diameter. **Figure 6*A*** shows an example of such a neuron with a spontaneous rate of 0.6 spikes/s. To analyze this relationship on a finer timescale, we calculated the spike-triggered average of the pupil diameter and found that this cell routinely spiked during constriction events (362 total spikes during a ~10 min recording period; **Fig. 6*B***). Across 43 silent-type CT cells that discharged a minimum of 5 spikes during the recording session, nearly all (91%; 39 of 43) showed a similar relationship between individual spikes and pupillary constriction, as verified by the negative pupil slope (**Fig. 6*C***). The average spike-triggered changes in pupil diameter from all recorded units indicate a similar effect, with spikes occurring during constriction events (n = 5243 spikes from 50 silent-type CT cells, recorded over 29090 s; **Fig. 6*D***). The relationship between pupil diameter and spiking activity was independent of preceding behavioral state, as we found qualitatively similar patterns of effects whether mice were sitting still or exhibiting exploratory movements (e.g., whisking or whisking/locomotion), suggesting silent-type CT cells are functioning during both quiet and active awake periods (data not shown). Thus, these data indicate that most spiking activity in silent-type CT cells occurs during pupillary constriction.

DISCUSSION

In this study, we have used the juxtacellular method to record optogenetically identified L6 CT neurons in wS1 of awake, head-restrained mice during periods of quiescence and whisker-related behavior. We characterized the modulation of CT spiking by behavioral state through continuous monitoring of arousal, whisking, and locomotion, making several novel observations. First, we found two subsets of CT cells that exhibited opposite changes in spiking rates as mice transition from quiet wakefulness to whisking: active-type and pausing-type. Second, some CT neurons, primarily the pausing-type, presented changes in firing rate well before whisking onset. Third, while arousal and whisking contribute to state-dependent changes in firing rates, we found that CT activity correlated more strongly and displayed better temporal alignment with EMG signals. Fourth, most L6 CT neurons in wS1 are spontaneously silent in the awake mouse, even during active whisking and locomotion. Finally, if they did spike, silent cells preferentially fired at the state transition point corresponding to when pupil diameter slowly constricted and the mouse entered a period of quiet wakefulness. Thus, our results demonstrate that L6 CT neurons in wS1 of awake mice have very diverse response properties and precisely timed responses around distinct state transition points.

Whisker-related responsive L6 CT neurons

Approximately one-third of L6 CT neurons encountered exhibited responses to whisker-related behavior. Because of their response properties, we differentiated this population into two types, an active-type with low spontaneous rates that increased spiking around whisking and a pausing-type with moderate spontaneous rates that decreased spiking

around whisking. These CT activity patterns are reminiscent of recent findings in other sensory cortices of *Ntsr1-Cre* mice during awake behavior (Augustinaite and Kuhn, 2020b; Clayton et al., 2021), suggesting a general feature of CT processing. However, naturally occurring transitions between distinct motor behaviors - whisking and locomotion - revealed heterogeneity within wS1. For example, we observed both phasic and tonic changes in firing rate during whisking associated with locomotion. Since mice begin whisking shortly before locomotion onset, phasic responses suggest that whisking and locomotion signals may have opposing effects on some CT cells. We also encountered a small subset of neurons active only during locomotion. Together, these results confirm that locomotion contributes to response diversity in wS1 (Sofroniew et al., 2015; Ayaz et al., 2019) and indicate that whisking and locomotion may have distinct roles in regulating the spontaneous spiking in CT circuits. Although they represent a minority of CT cells, these distinct whisker-related populations appear well-suited for dynamically regulating thalamocortical processing during sensorimotor behavior (Steriade, 2001).

One function of these CT cells may be to selectively enhance or suppress afferent sensory signals in a context-dependent manner. CT fibers from L6 are glutamatergic and thus a direct source of monosynaptic excitatory input to thalamic relay cells (Scharfman et al., 1990; Bourassa et al., 1995; Golshani et al., 2001), but they also indirectly inhibit them by recruiting GABAergic neurons in the thalamic reticular nucleus (TRN) (Cox et al., 1997; Kim et al., 1997; Golshani et al., 2001; Crandall et al., 2015). Previous work has shown that the sign of CT influence on thalamic relay cells is highly dynamic, with the excitatory-inhibitory balance shifting in an activity-dependent manner (von Krosigk et al., 1999; Crandall et al., 2015; Kirchgessner et al., 2020). During low-frequency activity, CT

effects are primarily suppressive, whereas higher-frequency activity yields enhancement. Thus, the activity of these two CT populations and perhaps their effects on thalamic excitability are complementary. For example, when active-type CT cells are firing at high rates during whisking, pausing-type cells are suppressed, and when active-type cells are firing at low frequencies in the absence of whisking, pausing-type cells spike at higher rates. Given L6 CT cells have diverse termination patterns across and within thalamic nuclei (Deschenes et al., 1998), future studies identifying the target of these CT cells will help to understand how these circuits control the spatial and temporal structure of thalamocortical activity during awake behavior (Temereanca and Simons, 2004; Crandall et al., 2015; Whitmire et al., 2016; Martinez-Garcia et al., 2020).

Premovement modulation of L6 CT activity

This study found that some active- and most pausing-type CT cells showed significant response modulation well before whisking onset. What might be the source of this premovement modulation in CT activity? One possibility is that the change in activity may involve recruiting neuromodulatory systems that control global arousal levels (Lee and Dan, 2012). Exploratory behaviors such as whisking and locomotion are closely associated with arousal and appear to be a substate of heightened arousal (McGinley et al., 2015b). Here we monitored pupil diameter to assay arousal (Reimer et al., 2014; McGinley et al., 2015a; Vinck et al., 2015), finding a strong correlation between the firing rates of whisker-related CT neurons and the time course of pupil dynamics. Consistent with recent reports in more superficial layers of wS1 and L6 CT cells in the visual cortex (Ayaz et al., 2019; Augustinaite and Kuhn, 2020b), we also observed the greatest firing

rate modulation occurring during whisking/locomotion. Although an increase in pupil diameter preceded whisking/locomotion, solitary whisking occurred before an increase in pupil diameter, suggesting that the modulation of L6 CT circuit activity may also represent a motor-preparatory signal. Consistent with this observation, we found stronger correlations and better temporal alignment between the firing rates of whisker-related CT cells and the time course of the EMG signal than pupil dynamics. Thus, the precisely timed modulation of some CT circuits in anticipation of voluntary whisking could provide context-dependent control of information processing in somatosensory thalamocortical circuits during awake behavior (Lee et al., 2008). Indeed, previous studies in rodents have shown that L6 wS1 neurons receive excitatory input from the whisker primary motor cortex (Zhang and Deschenes, 1998; Lee et al., 2008; Rocco-Donovan et al., 2011; Kinnischtzke et al., 2014; Kinnischtzke et al., 2016; Martinetti et al., 2021), a cortical area that appears to contribute directly to the initiation and modulation of whisking (Carvell et al., 1996; Sreenivasan et al., 2016). The enhancing and suppressive effects of such motor-preparatory signals on CT firing most likely depend on the engagement of specific excitatory and inhibitory mechanisms in L6 (Beierlein and Connors, 2002; Crandall et al., 2017; Frandolig et al., 2019; Martinetti et al., 2021).

Silent L6 CT neurons

Most L6 CT neurons (72%) in mouse wS1 exhibited little or no whisking/locomotion-related activity and had very low spontaneous firing rates. This proportion of “silent” cells is consistent with previous studies of antidromically identified CT neurons in S1 of sedated or anesthetized rats and awake rabbits (Landry and Dykes, 1985; Swadlow, 1989, 1990;

Swadlow and Hicks, 1996; Kelly et al., 2001; Lee et al., 2008; Kwegyir-Afful and Simons, 2009). Thus, there is considerable evidence across species and sensory modalities that many L6 CT neurons are fairly silent and unresponsive (Tsumoto and Suda, 1980; Swadlow, 1994; Beloozerova et al., 2003; Sirota et al., 2005; Stoelzel et al., 2017), even when animals are aroused and behaving, suggesting they are a common feature of CT systems. However, the function of this largely silent population is a mystery.

Here, we found that many of these neurons preferentially fired when the pupil diameter slowly constricted. Previous studies have shown that pupil constriction is associated with a decrease in cortical activation and an increase in the prevalence of low-frequency cortical oscillations (Reimer et al., 2014; McGinley et al., 2015a; Vinck et al., 2015), suggesting that silent CT neurons themselves may play a role in switching cortical network activity. So how does the sparse but precisely timed activity of a majority of excitatory L6 CT neurons impact cortical network activity? One possibility is synchronizing the output of translaminar L6 inhibitory cells (Olsen et al., 2012; Bortone et al., 2014), which could fire synchronously enough to reduce synaptic activity across all cortical layers, terminating cortical activation (Timofeev et al., 2001; Volgushev et al., 2006). Alternatively, synchronized low-frequency CT spiking could also serve to suppress the thalamus through the preferential recruitment of inhibitory TRN neurons (Crandall et al., 2015). Testing these predictions and further exploring the effects of different brain states on the spontaneous firing of CT cells will lead to additional insights into the functional significance of this mysterious population.

Indeed, considerable literature examining CT circuits describes diverse roles for L6 neurons in modulating sensory transmission. These functions include regulation of

gain or excitability (Olsen et al., 2012; Denman and Contreras, 2015; Guo et al., 2017; Wang et al., 2018; Ansorge et al., 2020), sharpening or shifting of sensory response properties (Temereanca and Simons, 2004; Andolina et al., 2007; Li and Ebner, 2007; Hasse and Briggs, 2017; Pauzin and Krieger, 2018; Pauzin et al., 2019; Voigts et al., 2020), enhancement of synchrony (Sillito et al., 1994; Contreras et al., 1996), regulation of sensory adaptation (Mease et al., 2014), and control of burst vs. tonic spiking (Wang et al., 2006; Kirchgessner et al., 2020). The current work complements these studies, and, together, they indicate that L6 CT cells are highly heterogeneous and likely have multiple modulatory functions.

Author contributions: S.D and S.R.C designed research; S.D and S.R.C performed research; D.M.A performed the histology; S.D analyzed the data; S.D. and S.R.C. wrote the paper.

Acknowledgments: This work was supported by NIH grants K99-NS096108 (to S.R.C) and R00-NS096108 (to S.R.C). We thank Barry Connors (Brown University) for generously providing the *Ntsr1-Cre* mice. We also thank the Michigan State University Center for Advanced Microscopy for confocal imaging support.

Conflict of interest: The authors declare no competing financial interests.

MATERIALS AND METHODS

Animals. All procedures were carried out in accordance with the National Institutes of Health (NIH) Guidelines for the Care and Use of Laboratory Animals and approved by the Michigan State University Institutional Animal Care and Use Committee (IACUC). The following mouse lines were used in this study: *Ntsr1-Cre* (MMRRC: 017266-UCD) (Gong et al., 2007), Ai32 (Jackson Labs: 024109) (Madisen et al., 2012), Ai14 (Jackson Labs: 007908) (Madisen et al., 2010), and Crl:CD1 (ICR: Charles River: 022). All *Ntsr1-Cre* mice used had Crl:CD1 genetic backgrounds. For most experiments, homozygous *Ntsr1-Cre* mice were crossed with a floxed ChR2 reporter line (homozygous Ai32), resulting in heterozygous experimental mice for the indicated genes. For viral injections, homozygous *Ntsr1-Cre* mice were crossed with Crl:CD1 mice. Experimental mice were group-housed with same-sex littermates before surgery and singly housed post-surgery in a dedicated animal care facility maintained on a reversed 12:12 h light-dark cycle. Food and water were available *ad libitum*. We used both male and female mice in this study.

*Surgical procedures and training***.** Mice were 6-60 weeks old at the time of surgery. Briefly, mice were anesthetized with a Ketamine-Dexdomitor mixture diluted in sterile saline (KetaVed, 100 mg/kg; Dexdomitor, 0.25 mg/kg; intraperitoneally). Once deeply anesthetized, we covered the eyes with a thin layer of ophthalmic ointment to prevent drying (Patterson Veterinary Artificial Tears). For chronic electromyography (EMG) recordings, fine Teflon-coated tungsten microwires (50 μm: A-M Systems # 795500) were first inserted under the skin into the left mystacial pad musculature, as previously described (Fee et al., 1997; Berg and Kleinfeld, 2003). The distal tips of wires (~1 mm) were stripped of insulation and hooked for stable positioning within the pad. The EMG

wire was then positioned on the head before the incised skin was closed with a surgical adhesive (GLUture). Mice were then placed into a digital stereotaxic frame with an integrated warming base that maintained core body temperature (Stoelting). Next, the skull was exposed using fine surgical scissors, the periosteum overlying the skull removed, and a small craniotomy (~0.75 mm diameter) made over the right wS1 (coordinates relative to bregma: 3.4 mm lateral and 1.1 mm posterior). A custom-built titanium head-post was then affixed to the skull with adhesive luting cement (C&B Metabond), and the resected skin closed around the outside of the head-post with tissue adhesive (GLUture). The EMG wire was attached to a gold pin (A-M Systems) with cold solder and secured in the luting cement. The craniotomy was then covered with Kwik-Cast (WPI), and Buprenorphine (0.05-0.1 mg/kg) was injected subcutaneously for postoperative pain relief. Mice were also given Antisedan (2.5 mg/kg) to reverse the effects of Dexdomitor. After surgery, mice were allowed to recover on a heating pad for 1-2 hours before returning to their home cage.

After 48-72 hours of recovery, implanted mice were handled and habituated to head fixation within the recording setup. We clamped the head-post to metal posts, positioned the mouse on a flexible circular treadmill, and then allowed mice to stand/walk/run freely in this position. Mice acclimated quickly to head fixation over the course of two 30-min sessions and ran naturally on the wheel, never showing signs of distress. Physiological recordings began once the animal was accustomed to head fixation, which was ~72 hours after surgery. All behavioral training and physiological recording were performed during the dark phase.

*Stereotactic Injections***.** For some mice (n = 2), an adeno-associated virus (AAV) that encoded Cre-dependent genes for hChR2(H134R)-EYFP fusion proteins was injected into the right wS1 during the head-posting procedure, as previously described (Crandall et al., 2015; Martinetti et al., 2021) (pAAV1.Ef1a.DIO.hChRr2(H134R)-eYFP.WPRE.hGH, Addgene: 20298-AAV1). Briefly, after the craniotomy was made over the wS1, a small volume of the virus was then pressure-ejected via a glass micropipette attached to a Picospritzer pressure system (0.33 μl over 10-15 min; titer = ~3.4 x 10^{12} viral genomes/ml). Viral solutions were injected between 0.8-1.0 mm ventral to pia surface. Following injection, the pipette was held in place for 10 min before withdrawal from the brain. After the procedure, mice were allowed to recover and express the viral vector for 10-12 days.

In Vivo Awake Recordings and Data Acquisition. On the day of recording, Kwik-cast was gently removed from the skull, exposing the craniotomy, and a drop of saline (0.9% NaCl) was placed on the skull to keep the exposed craniotomy moist. *In-vivo* juxtacellular recordings were achieved using borosilicate glass pipettes with tip resistances of 3-6 MΩ (tip diameter: 2-3 μm) when filled with HEPES-buffered artificial cerebrospinal fluid (ACSF) containing (in mM): 126 NaCl, 3 KCl, 5 HEPES, 1.25 NaH_2PO_4, 1 $MgSO_4$, 1.2 $CaCl_2$, 26 $NaHCO_3$, and 10 glucose, pH 7.25 with NaOH, osmolarity: 300 mOsm). Recording pipettes were mounted on a four-axis micromanipulator (Sutter Quad) and lowered through the craniotomy at a normal angle, avoiding blood vessels with guidance by stereomicroscope (Leica MZ10F). At a depth of 200-400 μm, the penetration was temporarily paused, and the craniotomy and pipette stabilized by applying warmed Agar or Agarose (3%) in saline (0.9% NaCl). The initial

speed of advancement was 5-10 μm/s, but manipulator advancement was slowed down to 2-4 μm/s at a depth of 800μm until a cell was encountered. During the search for a single cortical neuron, physiological activity and electrode resistance were monitored using Cambridge Electronic Design (CED) hardware and software and an audio amplifier (A-M Systems Model 3300). Upon detecting spontaneous or light-evoked (see below) small extracellular spikes, the recording pipette was slowly advanced until we could achieve a juxtacellular recording configuration. We defined this as a recording with spikes having a positive polarity initial phase and an increase in electrode resistance just before, or coincident with, the detection of a neuron. Juxtacellular recordings were considered for analysis if action potential amplitudes were ≥ 1 mV, remained stable throughout the recording, and if the series resistance varied ≤ 20%. We also included six neurons with extracellular spiking in the final dataset. The exclusion of these neurons from the dataset had no qualitative impact on the interpretation of results.

All electrophysiological and behavioral signals were acquired and digitized at 20 kHz using Cambridge Electronic Design hardware and software (Power 1401-3 and Signal 6). Juxtacellular data was obtained using a Multiclamp 700B amplifier (Molecular Devices), and signals were low pass filtered at 10 kHz before digitizing. During juxtacellular recordings, the pipette capacitances were neutralized, and series resistances (typically 10-25 MΩ) were compensated online. Series resistances were continually monitored during experiments to ensure sufficient compensation. The EMG electrode was connected to an A-M Systems preamplifier head-stage (20x) through a connector with small input leads, and then the voltage signals were further amplified 100x and band-pass filtered between 10 Hz to 3kHz using an A-M Systems 3600 amplifier.

Pupil signals were obtained from the eye contralateral to the recording site using a dedicated infrared (880 nm) eye-tracking system at a sampling rate of 120 Hz (ISCAN ETL-200 rodent series), and the output was interface via Cambridge Electronic Design hardware (Power 1401-3). An additional white LED was positioned above the mouse and provided low-intensity illumination such that the pupil was approximately mid-range in diameter when the animal was calm but alert. All recordings were performed in isoluminant conditions without any change in the ambient light during the course of a recording session. Locomotion epochs were tracked using an infrared emitting LED (940 nm) and an infrared-sensitive phototransistor (Sparkfun QRE1113).

In vivo Photostimulation and Identifying ChR2-expressing Neurons. We used local photostimulation to identify ChR2-expressing L6 CT neurons for *in vivo* recordings during awake behavior (Lima et al., 2009; Moore and Wehr, 2013; Munoz et al., 2014; Munoz et al., 2017; Yu et al., 2019). To couple light stimulation with juxtacellular recordings, we used a two-port glass pipette holder to insert an optical fiber into the recording pipette, providing direct illumination through the tip (A-M Systems, Optopatcher) (Katz et al., 2013). The internal optic fiber (0.22 NA, inner diameter of 200 μm, 1.25 mm OD ceramic ferrule, Thorlabs, FG200UCC) was positioned as deep as possible in the pipette to achieve maximum light intensity at the tip of the pipette (3-8 mW). The internal optic fiber was coupled to a 465 nm LED light source (Plexon, 94002-002) by a patch cable (0.22 NA, inner diameter of 200 μm, 1.25 mm OD ceramic ferrule, Thorlabs, M86L01) and driven by a single channel LED driver (Plexon, 51382). LED on/off times were fast (< 50 μs) and of constant amplitude and duration when verified with a fast photodiode (Thorlabs, DET36A).

While advancing the recording pipette, we used brief LED pulses (5 ms, Max LED intensity) delivered at low frequency (2 Hz) to identify putative ChR2-expressing neurons. Once a neuron was encountered and stable under the recording pipette, we ran a block of photostimulation trials (5 ms pulse duration, max intensity, >50 repetitions) to establish if the neuron expressed ChR2. After the photostimulation block, we recorded the neural activity simultaneously with other time-varying signals like EMG, pupil diameter, and locomotion. To confirm ChR2-expressing CT neurons offline, we focused our analysis on two characteristics: (1) the probability of light-evoked spikes and (2) the latency of peak light-evoked spikes.

In Vivo Juxtacellular Labeling. In a subset of experiments, we filled the juxtacellular recording pipette with HEPES-buffered ACSF containing 2.5% Neurobiotin (Vector Laboratories) so that the recorded cell could be labeled and subsequently identified (Pinault, 1996). Following the recording, we injected 5-15 nA positive current pulse (200-400 ms, 0.25 Hz) through the recording pipette to modulate the spiking activity. We continually monitored evoked spikes throughout the labeling protocol, and current amplitudes were adjusted to avoid increased spontaneous activity and cell damage. The recording pipette was slowly retracted once the labeling protocol was complete (typically 300-500 current pulses with evoked spikes). Following a survival period of 2-24 hrs, mice were sacrificed and brain tissue fixed for subsequent histology.

Histology and imaging. All tissue for histology was prepared from acute brain slices, as previously described (Crandall et al., 2017; Martinetti et al., 2021). Briefly, animals were anesthetized with isoflurane before being decapitated. Brains were removed and placed in a cold (~4°C) oxygenated (95% O_2, 5% CO_2) slicing solution

containing (in mM) 3 KCl, 1.25 NaH_2PO_4, 10 $MgSO_4$, 0.5 $CaCl_2$, 26 $NaHCO_3$, 10 glucose, and 234 sucrose. Brain slices (300-1000 μm thick) containing wS1 were cut using a vibrating tissue slicer (Leica VT1200S) and immediately transferred to a 4% paraformaldehyde in 0.1 M phosphate buffer solution overnight at 4°C (18 – 24 hr). The next day, slices were changed to a 30% sucrose in 0.1 M phosphate buffer solution until re-sectioned (4°C; 2 – 3 days). Individual brain slices were re-sectioned at 100 μm using a freezing microtome (Leica SM2010 R). Floating sections were washed twice in 0.1 M phosphate buffer followed by 3 washes in 0.1 M phosphate buffer with 0.15 M NaCl, pH 7.4 (PBS, 5 min per wash). After washing, sections were incubated for 1 hour at room temperature in a blocking solution containing 0.1% Tween, 0.25% Triton X-100, 10% normal goat serum in PBS. Sections were then incubated using Streptavidin/Biotin Blocking Kit (Vector Labs, Cat # SP-2002), 30 minutes in streptavidin solution, followed by 30 minutes in biotin solution with a brief rinse of PBS after each. Sections were then incubated with Alexa Fluor 568-conjugated streptavidin (Thermo- Fisher Scientific, Cat #S11226, 1:5000, 2μg/μl) solution made up in blocking solution for 3 hours with rotation at room temperature. Following incubation, sections were washed 3 times in PBS, then 2 times in 0.1 M phosphate buffer solution (10 min per wash), mounted, and cover-slipped using Vectashield with DAPI (Vector Laboratories H-1500). Fluorescent conjugates of streptavidin were stored and prepared as recommended by the manufacturer. Confocal image stacks of labeled neurons were taken using an Olympus FluoView 1000 filter-based Laser Scanning Confocal Microscope with a UPlanSApo (NA 1.40) 100x oil immersion objective and updated Version 4.2 software (laser excitation 405nm, 514nm, and 543nm). Image brightness and contrast were adjusted offline using Fiji software

(Schindelin et al., 2012). Three blinded independent observers examined cells to determine the presence or absence of membrane-bound ChR2-eYFP associated with the *in vivo* filled neurobiotin cells.

Electrophysiological Data Analysis. Electrophysiological and behavioral data were analyzed in Spike 2 (CED) and Matlab (Mathworks; Natick, MA). After the experiment, juxtacellular spiking data was high pass filtered (250-270 Hz, finite impulse filters (FIR) in Spike 2), and single action potentials (APs) were detected offline using Spike 2 software (CED). The spike identification procedure involved a two-step process of first setting a threshold with two trigger points (removing noise from putative spike) and then selecting a template from the recorded spike waveforms. Spike shapes with 60% of the points matching the pre-selected template were captured, added, and their event times saved. We then converted the timestamps of identified spikes and all other electrophysiological and behavioral data to Matlab files, and all subsequent analyses were performed using custom-written scripts in Matlab.

Briefly, we used spike timestamps to calculate the continuous instantaneous firing rate of the spike train. The instantaneous firing rate was calculated as the inverse of the inter-spike intervals and then smoothed with a low pass Butterworth filter of 100 ms window size, which we applied in both the forward and backward directions to ensure no net smearing of data in a particular direction. Next, the mystacial pad EMG signal was rectified and filtered with a 2nd order Butterworth filter with a desired final cut-off frequency of 5 Hz and applied in both forward and backward directions to avoid temporal smearing. The final signal was a continuous trace of the rectified EMG activity envelope during a recording session. The raw pupil diameter signal was also smoothed with a low pass

Butterworth filter with 100 ms window size, running forward and backward. Finally, the locomotion encoding output of the infrared phototransistor signal was rectified, differentiated, and low-pass filtered (5Hz) to get a smoothed locomotion signal.

The onset of locomotion and EMG epochs were calculated based on a threshold above the preceding baseline signal. All locomotion epochs, whisking epochs with or without locomotion, were initially detected manually. Once identified, we calculated the mean and standard deviation of the baseline as the average of the preceding 1 s of respective signals. We then defined locomotion onset objectively as the point +/- 500 ms around the manually detected onset that exceeded the baseline plus five times the standard deviation. Similarly, we defined whisking/EMG onset as the point exceeding baseline plus three times the standard deviation.

We extracted 5 s of data before and after each detected whisking/EMG onset for subsequent analysis of whisking with concomitant locomotion (whisking/locomotion) epochs. For a recorded neuron to be included for analysis, at least three locomotion epochs were needed. For whisking only (whisking) epochs, we extracted 3 s before and after each detected whisk. Every neuron considered in this study had greater than 10 such events. For statistical analysis of within neuron whisker-related modulation, baseline period was defined as: -4 s to -1 s before whisking onset for whisking/locomotion epochs, and -1.5 s to -0.5 s before whisking onset for solitary whisking episodes. The whisking period was defined as 3 s and 2 s starting from whisking onset for whisking/locomotion epochs and for solitary whisking epochs, respectively. For a neuron to be considered whisker-related, significant modulation ($p < 0.05$, Wilcoxon signed-rank test) from baseline for either whisking with or without locomotion epochs was needed.

To answer if whisker-related CT neurons were better correlated with whisking or a change in arousal, we cross-correlated instantaneous spiking activity with the time course of either the EMG signal or pupil dynamics. For whisking/locomotion epochs, we used 4 s of data centered on the whisking onset, whereas for solitary whisking, we used 3 s of data centered on whisking onset for cross-correlations. The analysis yielded correlation coefficients (r-value) at every time bin (of 1 ms) for lag and lead of 1 s each.

Statistical analysis. Statistical comparisons were performed in Matlab (Mathworks, Natick, MA). Details of specific comparisons are provided in the result section. Briefly, non-parametric tests were held as appropriate on most occasions based on a test of normality using the Shapiro-Wilk test. Paired and unpaired comparisons were performed using the Wilcoxon signed-rank test and the Mann-Whitney tests, respectively. All time-varying data traces (average instantaneous spike rates, EMG profile, and pupil dynamics) are represented as mean ± SEM, and any numerical representation (e.g., average spiking during a fixed time window and mean r-value) is represented as mean ± SD, and statistical significance was defined as $p < 0.05$. However, exact p-values are provided wherever applicable.

REFERENCES

Andolina IM, Jones HE, Wang W, Sillito AM (2007) Corticothalamic feedback enhances stimulus response precision in the visual system. Proc Natl Acad Sci USA 104:1685-1690.

Ansorge J, Humanes-Valera D, Pauzin FP, Schwarz MK, Krieger P (2020) Cortical layer 6 control of sensory responses in higher-order thalamus. J Physiol 598:3973-4001.

Augustinaite S, Kuhn B (2020a) Complementary Ca(2+) Activity of Sensory Activated and Suppressed Layer 6 Corticothalamic Neurons Reflects Behavioral State. Curr Biol 30:3945-3960 e3945.

Augustinaite S, Kuhn B (2020b) Complementary Ca(2+) Activity of Sensory Activated and Suppressed Layer 6 Corticothalamic Neurons Reflects Behavioral State. Curr Biol.

Ayaz A, Stauble A, Hamada M, Wulf MA, Saleem AB, Helmchen F (2019) Layer-specific integration of locomotion and sensory information in mouse barrel cortex. Nature communications 10:2585.

Beierlein M, Connors BW (2002) Short-term dynamics of thalamocortical and intracortical synapses onto layer 6 neurons in neocortex. J Neurophysiol 88:1924-1932.

Beloozerova IN, Sirota MG, Swadlow HA (2003) Activity of different classes of neurons of the motor cortex during locomotion. J Neurosci 23:1087-1097.

Berg RW, Kleinfeld D (2003) Rhythmic whisking by rat: retraction as well as protraction of the vibrissae is under active muscular control. J Neurophysiol 89:104-117.

Bortone DS, Olsen SR, Scanziani M (2014) Translaminar inhibitory cells recruited by layer 6 corticothalamic neurons suppress visual cortex. Neuron 82:474-485.

Bourassa J, Pinault D, Deschenes M (1995) Corticothalamic projections from the cortical barrel field to the somatosensory thalamus in rats: a single-fibre study using biocytin as an anterograde tracer. Eur J Neurosci 7:19-30.

Briggs F (2020) Role of Feedback Connections in Central Visual Processing. Annu Rev Vis Sci 6:313-334.

Briggs F, Usrey WM (2008) Emerging views of corticothalamic function. Curr Opin Neurobiol 18:403-407.

Briggs F, Usrey WM (2009) Parallel processing in the corticogeniculate pathway of the macaque monkey. Neuron 62:135-146.

Carvell GE, Miller SA, Simons DJ (1996) The relationship of vibrissal motor cortex unit activity to whisking in the awake rat. Somatosens Mot Res 13:115-127.

Clayton KK, Williamson RS, Hancock KE, Tasaka GI, Mizrahi A, Hackett TA, Polley DB (2021) Auditory Corticothalamic Neurons Are Recruited by Motor Preparatory Inputs. Curr Biol 31:310-321 e315.

Contreras D, Destexhe A, Sejnowski TJ, Steriade M (1996) Control of spatiotemporal coherence of a thalamic oscillation by corticothalamic feedback. Science 274:771-774.

Cox CL, Huguenard JR, Prince DA (1997) Nucleus reticularis neurons mediate diverse inhibitory effects in thalamus. Proc Natl Acad Sci USA 94:8854-8859.

Crandall SR, Cruikshank SJ, Connors BW (2015) A corticothalamic switch: controlling the thalamus with dynamic synapses. Neuron 86:768-782.

Crandall SR, Patrick SL, Cruikshank SJ, Connors BW (2017) Infrabarrels Are Layer 6 Circuit Modules in the Barrel Cortex that Link Long-Range Inputs and Outputs. Cell reports 21:3065-3078.

Cudeiro J, Sillito AM (2006) Looking back: corticothalamic feedback and early visual processing. Trends Neurosci 29:298-306.

Denman DJ, Contreras D (2015) Complex Effects on In Vivo Visual Responses by Specific Projections from Mouse Cortical Layer 6 to Dorsal Lateral Geniculate Nucleus. J Neurosci 35:9265-9280.

Deschenes M, Veinante P, Zhang ZW (1998) The organization of corticothalamic projections: reciprocity versus parity. Brain research Brain research reviews 28:286-308.

Diamond ME, von Heimendahl M, Knutsen PM, Kleinfeld D, Ahissar E (2008) 'Where' and 'what' in the whisker sensorimotor system. Nat Rev Neurosci 9:601-612.

Erisir A, Van Horn SC, Sherman SM (1997) Relative numbers of cortical and brainstem inputs to the lateral geniculate nucleus. Proc Natl Acad Sci USA 94:1517-1520.

Fee MS, Mitra PP, Kleinfeld D (1997) Central versus peripheral determinants of patterned spike activity in rat vibrissa cortex during whisking. J Neurophysiol 78:1144-1149.

Frandolig JE, Matney CJ, Lee K, Kim J, Chevee M, Kim SJ, Bickert AA, Brown SP (2019) The Synaptic Organization of Layer 6 Circuits Reveals Inhibition as a Major Output of a Neocortical Sublamina. Cell reports 28:3131-3143 e3135.

Gilbert CD, Wiesel TN (1979) Morphology and intracortical projections of functionally characterised neurones in the cat visual cortex. Nature 280:120-125.

Golshani P, Liu XB, Jones EG (2001) Differences in quantal amplitude reflect GluR4-subunit number at corticothalamic synapses on two populations of thalamic neurons. Proc Natl Acad Sci USA 98:4172-4177.

Gong S, Doughty M, Harbaugh CR, Cummins A, Hatten ME, Heintz N, Gerfen CR (2007) Targeting Cre recombinase to specific neuron populations with bacterial artificial chromosome constructs. J Neurosci 27:9817-9823.

Guo W, Clause AR, Barth-Maron A, Polley DB (2017) A Corticothalamic Circuit for Dynamic Switching between Feature Detection and Discrimination. Neuron 95:180-194 e185.

Hasse JM, Briggs F (2017) Corticogeniculate feedback sharpens the temporal precision and spatial resolution of visual signals in the ferret. Proc Natl Acad Sci USA 114:E6222-E6230.

Katz Y, Yizhar O, Staiger J, Lampl I (2013) Optopatcher--an electrode holder for simultaneous intracellular patch-clamp recording and optical manipulation. J Neurosci Methods 214:113-117.

Kelly MK, Carvell GE, Hartings JA, Simons DJ (2001) Axonal conduction properties of antidromically identified neurons in rat barrel cortex. Somatosens Mot Res 18:202-210.

Kim J, Matney CJ, Blankenship A, Hestrin S, Brown SP (2014) Layer 6 corticothalamic neurons activate a cortical output layer, layer 5a. J Neurosci 34:9656-9664.

Kim T, Thankachan S, McKenna JT, McNally JM, Yang C, Choi JH, Chen L, Kocsis B, Deisseroth K, Strecker RE, Basheer R, Brown RE, McCarley RW (2015) Cortically projecting basal forebrain parvalbumin neurons regulate cortical gamma band oscillations. Proc Natl Acad Sci USA 112:3535-3540.

Kim U, Sanchez-Vives MV, McCormick DA (1997) Functional dynamics of GABAergic inhibition in the thalamus. Science 278:130-134.

Kinnischtzke AK, Simons DJ, Fanselow EE (2014) Motor cortex broadly engages excitatory and inhibitory neurons in somatosensory barrel cortex. Cerebral cortex 24:2237-2248.

Kinnischtzke AK, Fanselow EE, Simons DJ (2016) Target-specific M1 inputs to infragranular S1 pyramidal neurons. J Neurophysiol 116:1261-1274.

Kirchgessner MA, Franklin AD, Callaway EM (2020) Context-dependent and dynamic functional influence of corticothalamic pathways to first- and higher-order visual thalamus. Proc Natl Acad Sci USA 117:13066-13077.

Kwegyir-Afful EE, Simons DJ (2009) Subthreshold receptive field properties distinguish different classes of corticothalamic neurons in the somatosensory system. J Neurosci 29:964-972.

Landry P, Dykes RW (1985) Identification of two populations of corticothalamic neurons in cat primary somatosensory cortex. Exp Brain Res 60:289-298.

Lee S, Carvell GE, Simons DJ (2008) Motor modulation of afferent somatosensory circuits. Nat Neurosci 11:1430-1438.

Lee SH, Dan Y (2012) Neuromodulation of brain states. Neuron 76:209-222.

Li L, Ebner FF (2007) Cortical modulation of spatial and angular tuning maps in the rat thalamus. J Neurosci 27:167-179.

Lima SQ, Hromadka T, Znamenskiy P, Zador AM (2009) PINP: a new method of tagging neuronal populations for identification during in vivo electrophysiological recording. PloS one 4:e6099.

Liu XB, Honda CN, Jones EG (1995) Distribution of four types of synapse on physiologically identified relay neurons in the ventral posterior thalamic nucleus of the cat. J Comp Neurol 352:69-91.

Madisen L, Zwingman TA, Sunkin SM, Oh SW, Zariwala HA, Gu H, Ng LL, Palmiter RD, Hawrylycz MJ, Jones AR, Lein ES, Zeng H (2010) A robust and high-throughput

Cre reporting and characterization system for the whole mouse brain. Nat Neurosci 13:133-140.

Madisen L et al. (2012) A toolbox of Cre-dependent optogenetic transgenic mice for light-induced activation and silencing. Nat Neurosci 15:793-802.

Martinetti LE, Bonekamp KE, Autio DM, Kim HH, Crandall SR (2021) Short-Term Facilitation of Long-Range Corticocortical Synapses Revealed by Selective Optical Stimulation. Cerebral cortex.

Martinez-Garcia RI, Voelcker B, Zaltsman JB, Patrick SL, Stevens TR, Connors BW, Cruikshank SJ (2020) Two dynamically distinct circuits drive inhibition in the sensory thalamus. Nature 583:813-818.

McGinley MJ, David SV, McCormick DA (2015a) Cortical Membrane Potential Signature of Optimal States for Sensory Signal Detection. Neuron 87:179-192.

McGinley MJ, Vinck M, Reimer J, Batista-Brito R, Zagha E, Cadwell CR, Tolias AS, Cardin JA, McCormick DA (2015b) Waking State: Rapid Variations Modulate Neural and Behavioral Responses. Neuron 87:1143-1161.

Mease RA, Krieger P, Groh A (2014) Cortical control of adaptation and sensory relay mode in the thalamus. Proc Natl Acad Sci USA 111:6798-6803.

Moore AK, Wehr M (2013) Parvalbumin-expressing inhibitory interneurons in auditory cortex are well-tuned for frequency. J Neurosci 33:13713-13723.

Munoz W, Tremblay R, Rudy B (2014) Channelrhodopsin-assisted patching: in vivo recording of genetically and morphologically identified neurons throughout the brain. Cell reports 9:2304-2316.

Munoz W, Tremblay R, Levenstein D, Rudy B (2017) Layer-specific modulation of neocortical dendritic inhibition during active wakefulness. Science 355:954-959.

Olsen SR, Bortone DS, Adesnik H, Scanziani M (2012) Gain control by layer six in cortical circuits of vision. Nature 483:47-52.

Pauzin FP, Krieger P (2018) A Corticothalamic Circuit for Refining Tactile Encoding. Cell reports 23:1314-1325.

Pauzin FP, Schwarz N, Krieger P (2019) Activation of Corticothalamic Layer 6 Cells Decreases Angular Tuning in Mouse Barrel Cortex. Frontiers in neural circuits 13:67.

Petersen CCH (2019) Sensorimotor processing in the rodent barrel cortex. Nat Rev Neurosci 20:533-546.

Pinault D (1996) A novel single-cell staining procedure performed in vivo under electrophysiological control: morpho-functional features of juxtacellularly labeled thalamic cells and other central neurons with biocytin or Neurobiotin. J Neurosci Methods 65:113-136.

Reimer J, Froudarakis E, Cadwell CR, Yatsenko D, Denfield GH, Tolias AS (2014) Pupil Fluctuations Track Fast Switching of Cortical States during Quiet Wakefulness. Neuron 84:355-362.

Rocco-Donovan M, Ramos RL, Giraldo S, Brumberg JC (2011) Characteristics of synaptic connections between rodent primary somatosensory and motor cortices. Somatosens Mot Res 28:63-72.

Scharfman HE, Lu SM, Guido W, Adams PR, Sherman SM (1990) N-methyl-D-aspartate receptors contribute to excitatory postsynaptic potentials of cat lateral geniculate neurons recorded in thalamic slices. Proc Natl Acad Sci USA 87:4548-4552.

Schindelin J, Arganda-Carreras I, Frise E, Kaynig V, Longair M, Pietzsch T, Preibisch S, Rueden C, Saalfeld S, Schmid B, Tinevez JY, White DJ, Hartenstein V, Eliceiri K, Tomancak P, Cardona A (2012) Fiji: an open-source platform for biological-image analysis. Nat Methods 9:676-682.

Sherman SM, Koch C (1986) The control of retinogeniculate transmission in the mammalian lateral geniculate nucleus. Exp Brain Res 63:1-20.

Sillito AM, Jones HE, Gerstein GL, West DC (1994) Feature-linked synchronization of thalamic relay cell firing induced by feedback from the visual cortex. Nature 369:479-482.

Simons DJ (1978) Response properties of vibrissa units in rat SI somatosensory neocortex. J Neurophysiol 41:798-820.

Sirota MG, Swadlow HA, Beloozerova IN (2005) Three channels of corticothalamic communication during locomotion. J Neurosci 25:5915-5925.

Sofroniew NJ, Cohen JD, Lee AK, Svoboda K (2014) Natural whisker-guided behavior by head-fixed mice in tactile virtual reality. J Neurosci 34:9537-9550.

Sofroniew NJ, Vlasov YA, Andrew Hires S, Freeman J, Svoboda K (2015) Neural coding in barrel cortex during whisker-guided locomotion. eLife 4.

Sreenivasan V, Esmaeili V, Kiritani T, Galan K, Crochet S, Petersen CC (2016) Movement Initiation Signals in Mouse Whisker Motor Cortex. Neuron 92:1368-1382.

Steriade M (2001) Impact of network activities on neuronal properties in corticothalamic systems. J Neurophysiol 86:1-39.

Stoelzel CR, Bereshpolova Y, Alonso JM, Swadlow HA (2017) Axonal Conduction Delays, Brain State, and Corticogeniculate Communication. J Neurosci 37:6342-6358.

Swadlow HA (1989) Efferent neurons and suspected interneurons in S-1 vibrissa cortex of the awake rabbit: receptive fields and axonal properties. J Neurophysiol 62:288-308.

Swadlow HA (1990) Efferent neurons and suspected interneurons in S-1 forelimb representation of the awake rabbit: receptive fields and axonal properties. J Neurophysiol 63:1477-1498.

Swadlow HA (1994) Efferent neurons and suspected interneurons in motor cortex of the awake rabbit: axonal properties, sensory receptive fields, and subthreshold synaptic inputs. J Neurophysiol 71:437-453.

Swadlow HA, Weyand TG (1987) Corticogeniculate neurons, corticotectal neurons, and suspected interneurons in visual cortex of awake rabbits: receptive-field properties, axonal properties, and effects of EEG arousal. J Neurophysiol 57:977-1001.

Swadlow HA, Hicks TP (1996) Somatosensory cortical efferent neurons of the awake rabbit: latencies to activation via supra--and subthreshold receptive fields. J Neurophysiol 75:1753-1759.

Temereanca S, Simons DJ (2004) Functional topography of corticothalamic feedback enhances thalamic spatial response tuning in the somatosensory whisker/barrel system. Neuron 41:639-651.

Timofeev I, Grenier F, Steriade M (2001) Disfacilitation and active inhibition in the neocortex during the natural sleep-wake cycle: an intracellular study. Proc Natl Acad Sci USA 98:1924-1929.

Tsumoto T, Suda K (1980) Three groups of cortico-geniculate neurons and their distribution in binocular and monocular segments of cat striate cortex. J Comp Neurol 193:223-236.

Van Horn SC, Erisir A, Sherman SM (2000) Relative distribution of synapses in the A-laminae of the lateral geniculate nucleus of the cat. J Comp Neurol 416:509-520.

Velez-Fort M, Bracey EF, Keshavarzi S, Rousseau CV, Cossell L, Lenzi SC, Strom M, Margrie TW (2018) A Circuit for Integration of Head- and Visual-Motion Signals in Layer 6 of Mouse Primary Visual Cortex. Neuron 98:179-191 e176.

Vinck M, Batista-Brito R, Knoblich U, Cardin JA (2015) Arousal and locomotion make distinct contributions to cortical activity patterns and visual encoding. Neuron 86:740-754.

Voigts J, Deister CA, Moore CI (2020) Layer 6 ensembles can selectively regulate the behavioral impact and layer-specific representation of sensory deviants. eLife 9.

Volgushev M, Chauvette S, Mukovski M, Timofeev I (2006) Precise long-range synchronization of activity and silence in neocortical neurons during slow-wave oscillations [corrected]. J Neurosci 26:5665-5672.

von Krosigk M, Monckton JE, Reiner PB, McCormick DA (1999) Dynamic properties of corticothalamic excitatory postsynaptic potentials and thalamic reticular inhibitory postsynaptic potentials in thalamocortical neurons of the guinea-pig dorsal lateral geniculate nucleus. Neuroscience 91:7-20.

Wang W, Jones HE, Andolina IM, Salt TE, Sillito AM (2006) Functional alignment of feedback effects from visual cortex to thalamus. Nat Neurosci 9:1330-1336.

Wang W, Andolina IM, Lu Y, Jones HE, Sillito AM (2018) Focal Gain Control of Thalamic Visual Receptive Fields by Layer 6 Corticothalamic Feedback. Cerebral cortex 28:267-280.

White EL, Keller A (1987) Intrinsic circuitry involving the local axon collaterals of corticothalamic projection cells in mouse SmI cortex. J Comp Neurol 262:13-26.

Whitmire CJ, Waiblinger C, Schwarz C, Stanley GB (2016) Information Coding through Adaptive Gating of Synchronized Thalamic Bursting. Cell reports 14:795-807.

Winer JA, Diehl JJ, Larue DT (2001) Projections of auditory cortex to the medial geniculate body of the cat. J Comp Neurol 430:27-55.

Yu J, Hu H, Agmon A, Svoboda K (2019) Recruitment of GABAergic Interneurons in the Barrel Cortex during Active Tactile Behavior. Neuron 104:412-427 e414.

Zhang ZW, Deschenes M (1997) Intracortical axonal projections of lamina VI cells of the primary somatosensory cortex in the rat: a single-cell labeling study. J Neurosci 17:6365-6379.

Zhang ZW, Deschenes M (1998) Projections to layer VI of the posteromedial barrel field in the rat: a reappraisal of the role of corticothalamic pathways. Cerebral cortex 8:428-436.

FIGURE LEGENDS

Figure 1. Optogenetic tagging and functional identification of genetically defined L6 CT neurons in wS1 of the *Ntsr1-Cre* driver mouse line. ***A,*** Left: Confocal image of a fixed brain section (40 μm), centered on wS1, from an *Ntsr1-Cre* x floxed-tdTomato reporter (Ai14) mouse. White arrowheads indicate Ntsr1 expressing CT somata in L6. Right: Confocal image from the same fixed section, centered on the somatosensory thalamus, showing tdTomato-labeled CT axons terminating densely (VPm: ventral posterior medial nucleus; POm: posterior medial nucleus; TRN: thalamic reticular nucleus). The tissue was stained immunohistochemically for NeuN (blue). ***B,*** Schematic of the experimental setup. Head-fixed *Ntsr1-Cre* x floxed-ChR2-EYFP reporter (Ai32) mice stood or walked/ran on a flexible circular treadmill during juxtacellular recordings from neurons in wS1 while simultaneously monitoring mystacial pad EMG, pupil diameter, and locomotion. We used an optical fiber located inside the glass recording pipette to deliver blue light locally through the tip for stimulation and identification of ChR2-expressing L6 CT cells *in vivo* (optogenetic tagging; 465 nm LED). ***C,*** Top: Raster plot of light-evoked spiking (blue dots) order by trial number for a ChR2-expressing L6 CT neuron. Brief LED flashes (5 ms) from the pipette tip evoked reliable spikes with short onset latencies (blue voltage trace) across all trials (grey traces). Bottom: Peristimulus time histogram (PSTH) of spike probability for 64 trials aligned on LED onset (blue line) (bin size: 1 ms). For this neuron, we observed reliable light-evoked spikes within 2 ms of LED onset. ***D,*** Post hoc confocal images of the same neuron (shown in C) labeled with neurobiotin by *in vivo* juxtacellular methods during the recording. Membrane ChR2-EYFP expression histologically confirmed that this recorded cell was a ChR2-expressing L6 CT neuron in the *Ntsr1* x Ai32 mouse. ***E,*** The normalized spike probability of all optogenetically tagged L6 CT neurons during brief photostimulation (n = 115 cells from 27 mice), sorted by mean spike probability in the 5 ms after LED onset. The white line indicates LED onset. ***F,*** Left: Example of an average spike waveform recorded from a directly photoactivated L6 CT neuron (blue) and of a putative fast-spiking (FS) interneuron (black) recruited by the phototactivation of nearby L6 CT cells. Middle: Plot showing the separation of putative FS interneurons from L6 CT cells based on the peak-to-trough duration and the peak-to-trough ratio of their average recorded spike waveform. Right: Plot showing that light-evoked response of L6 CT cells

also exhibited greater spike probability and shorter latency to peak spiking probability than putative FS interneurons.

Figure 2. L6 CT neuron spiking as a function of behavioral state in awake, head-fixed mice. ***A,*** Example data from one juxtacellularly recorded L6 CT neuron across arousal and whisking states with low spiking rates (silent-type L6 CT) during both quiet awake periods and self-initiated whisker-related behavior (grey shadings). The mean firing rate for this cell was 0.012 spikes/s across the entire recording session. Instantaneous firing rate is shown, together with rectified EMG of the contralateral mystacial pad musculature, pupil diameter, and walking patterns on the same time base. The instantaneous firing rate and pupil diameter were smoothed with a low pass Butterworth filter in both directions (100 ms window). Pupil diameter was monitored to assess global arousal levels. ***B,*** Example data from one juxtacellularly recorded L6 CT neuron across arousal and whisking states with enhanced spiking rates (active-type L6 CT) during self-initiated whisker-related behavior (grey shadings). ***C,*** Example data from one juxtacellularly recorded L6 CT neuron across arousal and whisking states with suppressed spiking rates (pausing-type L6 CT) during self-initiated whisker-related behavior (grey shadings).

Figure 3. Diverse response profiles exhibited by whisker-related L6 CT neurons in wS1. ***A,*** Examples of juxtacellular unit responses recorded from individual L6 CT neurons displayed as raster plots and PSTHs aligned on EMG onset (red dashed line; time = 0) during whisking/locomotion. The first four examples (left to right) show active-type CT neurons, whereas the last two are pausing-type CT cells. Active-type CT neurons had either tonic firing at EMG onset (left), phasic increases in activity at EMG onset (second from left), a slow build-up of activity preceding EMG onset (third from left), or delayed increases in activity from EMG onset (fourth from left). Pausing-type CT neurons showed less diversity and tended to have decreased spiking rates before EMG onset. For the PSTHs, neural activity (black line) and EMG activity (red line) are plotted as mean ± SEM (grey shadow indicating SEM). ***B,*** Juxtacellular unit responses for the same CT neurons (shown in A) displayed as raster plots and PSTHs aligned on EMG onset (red dashed line; time = 0) during whisking. We found that most CT cells were modulated during

solitary whisking similarly to whisking/locomotion. The only exception were cells that had delayed increases in activity during locomotion (i.e., the fourth cell from left), which did not respond during whisking. ***C,*** Left: The spiking patterns of all whisker-related wS1 L6 CT neurons aligned on the EMG onset during whisking/locomotion. Each row is a neuron normalized to maximum firing rate and sorted by the mean baseline activity (3 s preceding EMG onset; white line; time = 0). Sorting neurons according to their baseline spiking before EMG onset with whisking/locomotion revealed L6 CT neurons that were active (active-type, top rows) and suppressed during whisking/locomotion (pausing-type, bottom rows). Right: The spiking patterns of all whisker-related L6 CT neurons aligned on the EMG onset during whisking. Neurons are sorted in the same order as in C, left. **D,** Summary graphs of spiking activity for all activity-type L6 CT cells. Top: Mean firing rate during whisking/locomotion (red circles) and solitary whisking (blue circles), plotted as a function of mean baseline activity preceding EMG onset (n = 19 cells; p = 2.44e-04 and 4.88e-04, respectively; Wilcoxon signed-rank test). The filled circles represent means. Bottom: Peak firing rate for each neuron during whisking/locomotion plotted as a function of peak activity during whisking (p = 2.44e-04; Wilcoxon signed-rank test). **E,** Summary graphs of spiking activity for all pausing-type L6 CT cells. Top: Mean firing rate during whisking/locomotion (red circles) and whisking (blue circles), plotted as a function of mean baseline activity preceding EMG onset (n = 13 cells; p = 0.03 and 4.88e-04, respectively; Wilcoxon signed-rank test). The filled circles represent means. Bottom: Trough (lowest) firing rate for each neuron during whisking/locomotion plotted against that for whisking (p = 2.44e-04, Wilcoxon sign-rank test).

Figure 4: Subpopulations of whisker-related L6 CT cells are modulated before whisker movement. ***A,*** Top: Two active-type L6 CT neurons exhibiting pre-EMG spike enhancement. Bottom: Two pausing-type L6 CT neurons exhibiting pre-EMG spike suppression. The red and black vertical dashed lines indicate EMG onset and the detected whisker-related spike modulation, respectively. ***B,*** Shown are the onset latencies of the pre-EMG spiking modulation for 5 active- and 10 pausing-type L6 CT neurons with a mean baseline firing rate greater than 2 spikes/s before whisking/locomotion. Most active-type CT cells (8 of 13) had little or no baseline firing

rate, rendering them unsuitable for analysis (see text). In contrast, most pausing-type CT neurons (9 of 10) exhibited pre-EMG spiking suppression. ***C,*** Shown are the onset latencies of the pre-EMG spiking modulation for 7 active and 10 pausing-type L6 CT neurons with a mean baseline firing rate greater than 2 spikes/s before solitary whisking episodes. Similar to B, most pausing-type CT neurons and some active-type CT neurons exhibited pre-EMG spiking modulation. ***D,*** Averages of mean normalized pupil diameter and mean locomotion activity of all locomotion bouts for each neuron. Data is aligned on the onset of locomotion across all sessions when a whisker-related neuron was recorded (n = 32 sessions). Pupil diameter was normalized to maximum dilation during the session. Values are represented as mean ± SEM. ***E,*** Averages of mean EMG and mean pupil diameter during whisking/locomotion (same data shown in D) but now aligned on EMG onset. Values are represented as mean ± SEM. ***F,*** Averages of mean EMG and mean normalized pupil diameter during whisking aligned on EMG onset across all sessions (n = 32 sessions). Pupil modulation occurs after EMG onset. Values are represented as mean ± SEM.

Figure 5. Contributions of whisking and arousal to L6 CT neuron in wS1 of awake mice. ***A-B,*** Cross-correlograms of spiking activity and EMG signals (top, red) or pupil dynamics (bottom, blue) from active-type (***A***) and pausing-type CT neurons (***B***) during whisking/locomotion (left) and whisking (right). Light-colored lines (red and blue) represent the average trial-by-trial cross-correlations for each whisker-related CT neuron. The dark-colored lines (red and blue) represent the mean cross-correlation across all neurons (n = 13/13 active-type cells; n = 11/12 pausing-type cells for whisking/locomotion and whisking, respectively). ***C-D,*** Left, summary graphs showing the absolute peak cross-correlation of pupil dynamics to firing activity as a function of the peak cross-correlation of EMG and firing activity for each active- (***C***, left) and pausing-type CT cell (***D***, left) during whisking/locomotion (black circles) and whisking (grey circles). Right, summary graphs showing the comparison of lags at which peak absolute correlation coefficients were obtained for active- (***C,*** right) and pausing-type CT neurons (***D,*** right) during whisking/locomotion and whisking (Active-type mean cross-correlation values: EMG during whisking/locomotion = 0.56 ± 0.20; Pupil during whisking/locomotion = 0.51 ± 0.21;

EMG during whisking = 0.31 ± 0.16; Pupil during whisking = 0.22 ± 0.12) (Pausing-type mean cross-correlation values: EMG during whisking/locomotion = 0.56 ± 0.17; Pupil during whisking/locomotion = 0.50 ± 0.16; EMG during whisk-only = 0.27 ± 0.16; Pupil during whisk-only = 0.23 ± 0.17). All statistical comparisons were performed with Wilcoxon paired signed-rank test (Active-type CT cells: during whisking/locomotion: p = 0.06; whisking: p = 2.44e-04; Pausing-type CT cells: during whisking/locomotion: p = 0.002; whisking: p = 0.27). Data in ***C*** (right) and ***D*** (right) are plotted as median, interquartile distance, and range (Active-type CT cells: during whisking/locomotion: p = 0.002; whisking: p = 2.44e-04; Pausing-type CT cells: during whisking/locomotion: p = 0.002; whisking: p = 0.08; Wilcoxon paired signed-rank test).

Figure 6. Silent L6 CT cells in wS1 preferentially fired during pupil constrictions. *A,* Pupil diameter (black trace) and spike times (grey ticks) are shown as a function of recording time for a silent L6 CT cell. Insets, expansion in time showing the relationship between spiking and pupil diameter (1, 2, and 3; grey shading). Note the increased incidence of spikes during pupil constriction. ***B,*** Spike-triggered pupil average for the same pupil cell pair (shown in **A**). Left: Raw pupil traces aligned on spike onset (n = 362 spikes; time = 0, dotted vertical line). It is hard to appreciate any trends in pupillary responses as they spanned a broad range of pupil diameters. For better visualization, we normalized the extracted pupillary responses to the peak of each extracted pupillary response Middle: The same spike-aligned pupil traces normalized to their peak value. Note the clear tendency of preceding pupil constriction in most instances just before spiking. Right: Mean and SEM of the normalized spike-triggered pupil (black line and grey shadow). ***C,*** The normalized spike-triggered pupil average for each silent wS1 L6 CT neuron (n = 43 cells; similar to B, right panel). Only CT cells with more than five spikes recorded in the entire session were used for analysis (7 cells excluded with < 5spikes). ***D,*** Mean and SEM of all normalized spike-triggered pupil traces (n = 5243 traces) across all the silent CT cells (n = 50 cells). Values are represented as mean ± SEM.

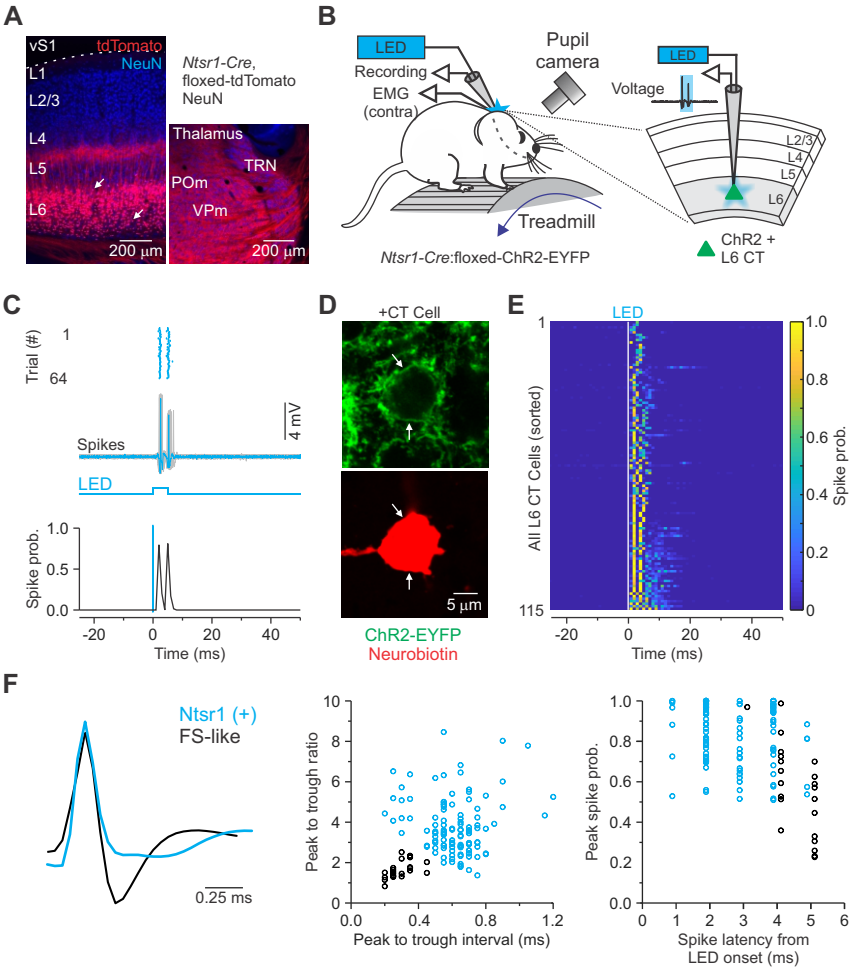
A
vS1
tdTomato
NeuN
L1
L2/3
L4
L5
L6
200 µm
Ntsr1-Cre,
floxed-tdTomato
NeuN
Thalamus
TRN
POm
VPm
200 µm
B
LED
Recording
EMG
(contra)
Pupil
camera
LED
Voltage
L2/3
L4
L5
L6
Treadmill
Ntsr1-Cre:floxed-ChR2-EYFP
ChR2 +
L6 CT
C
Trial (#)
1
64
Spikes
4 mV
LED
Spike prob.
1.0
0.5
0.0
-20
0
20
40
Time (ms)
D
+CT Cell
5 µm
ChR2-EYFP
Neurobiotin
E
LED
1
115
All L6 CT Cells (sorted)
-20
0
20
40
Time (ms)
1.0
0.8
0.6
0.4
0.2
0
Spike prob.
F
Ntsr1 (+)
FS-like
0.25 ms
Peak to trough ratio
Peak to trough interval (ms)
Peak spike prob.
Spike latency from
LED onset (ms)

Figure 1

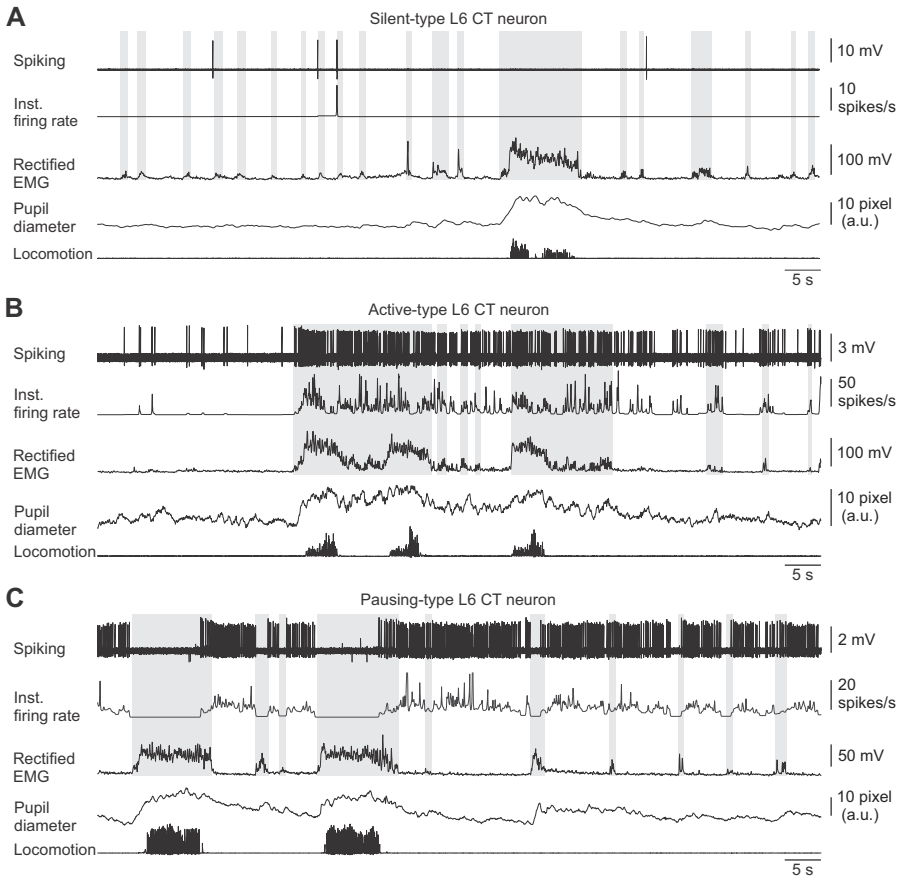
A
Silent-type L6 CT neuron
Spiking
Inst.
firing rate
Rectified
EMG
Pupil
diameter
Locomotion
10 mV
10
spikes/s
100 mV
10 pixel
(a.u.)
5 s
B
Active-type L6 CT neuron
Spiking
Inst.
firing rate
Rectified
EMG
Pupil
diameter
Locomotion
3 mV
50
spikes/s
100 mV
10 pixel
(a.u.)
5 s
C
Pausing-type L6 CT neuron
Spiking
Inst.
firing rate
Rectified
EMG
Pupil
diameter
Locomotion
2 mV
20
spikes/s
50 mV
10 pixel
(a.u.)
5 s

Figure 2

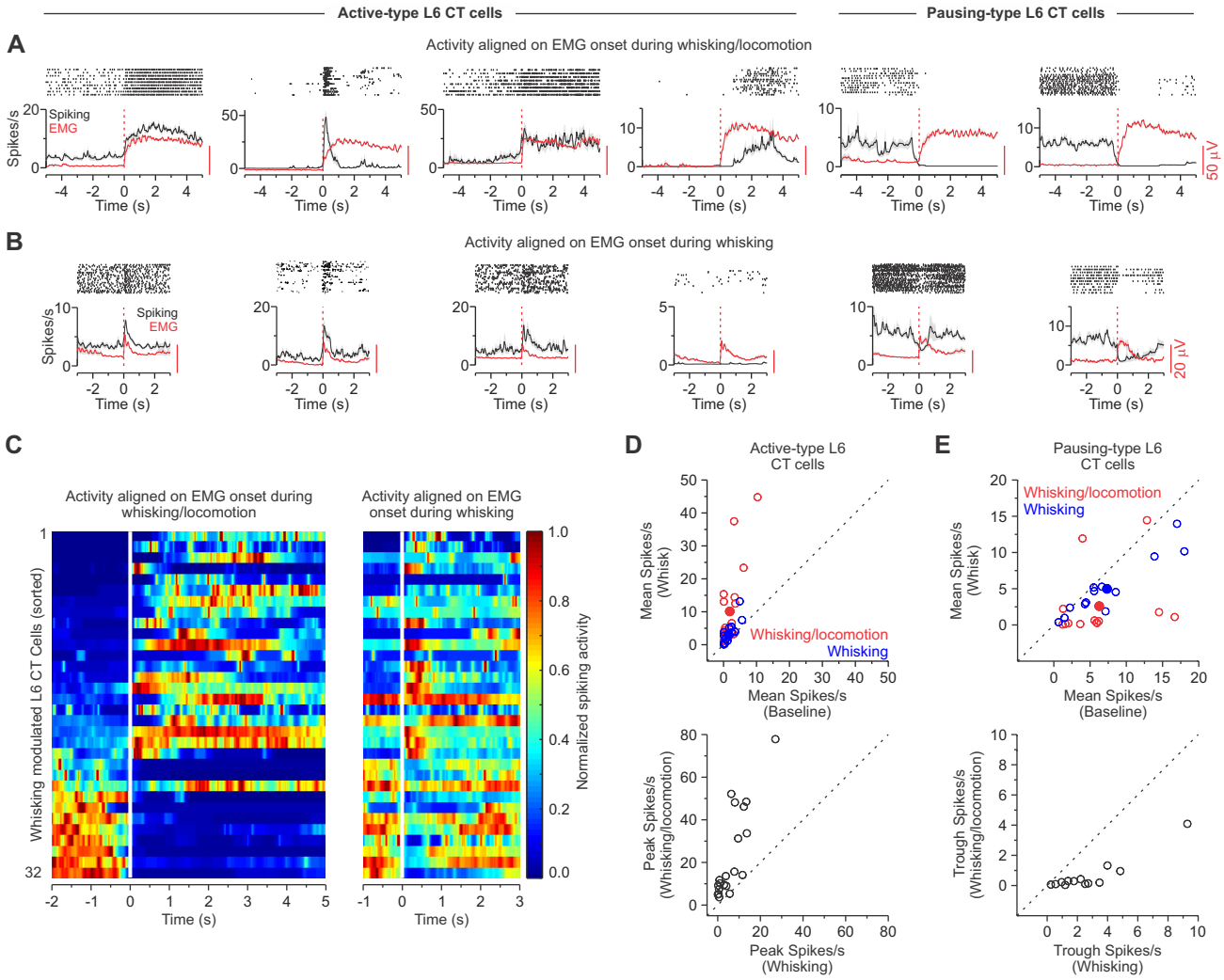
Active-type L6 CT cells
Pausing-type L6 CT cells
A
Activity aligned on EMG onset during whisking/locomotion
Spiking
EMG
Spikes/s
Time (s)
50 µV
B
Activity aligned on EMG onset during whisking
20 µV
C
Activity aligned on EMG onset during whisking/locomotion
Activity aligned on EMG onset during whisking
Whisking modulated L6 CT Cells (sorted)
Normalized spiking activity
D
Active-type L6 CT cells
Mean Spikes/s (Whisk)
Mean Spikes/s (Baseline)
Whisking/locomotion
Whisking
Peak Spikes/s (Whisking/locomotion)
Peak Spikes/s (Whisking)
E
Pausing-type L6 CT cells
Trough Spikes/s (Whisking/locomotion)
Trough Spikes/s (Whisking)

Figure 3

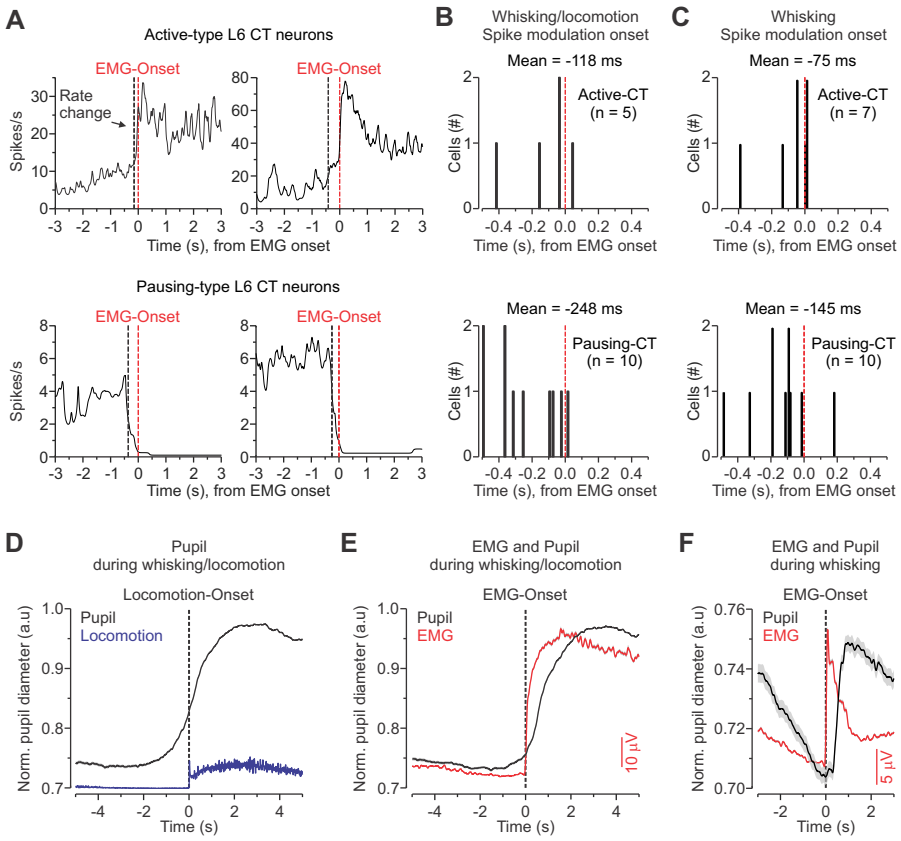
A
Active-type L6 CT neurons
EMG-Onset
EMG-Onset
Rate change
Spikes/s
Time (s), from EMG onset
Pausing-type L6 CT neurons
EMG-Onset
EMG-Onset
Spikes/s
Time (s), from EMG onset
B
Whisking/locomotion
Spike modulation onset
Mean = -118 ms
Active-CT (n = 5)
Cells (#)
Time (s), from EMG onset
Mean = -248 ms
Pausing-CT (n = 10)
Cells (#)
Time (s), from EMG onset
C
Whisking
Spike modulation onset
Mean = -75 ms
Active-CT (n = 7)
Cells (#)
Time (s), from EMG onset
Mean = -145 ms
Pausing-CT (n = 10)
Cells (#)
Time (s), from EMG onset
D
Pupil
during whisking/locomotion
Locomotion-Onset
Pupil
Locomotion
Norm. pupil diameter (a.u)
Time (s)
E
EMG and Pupil
during whisking/locomotion
EMG-Onset
Pupil
EMG
10 µV
Norm. pupil diameter (a.u)
Time (s)
F
EMG and Pupil
during whisking
EMG-Onset
Pupil
EMG
5 µV
Norm. pupil diameter (a.u)
Time (s)

Figure 4

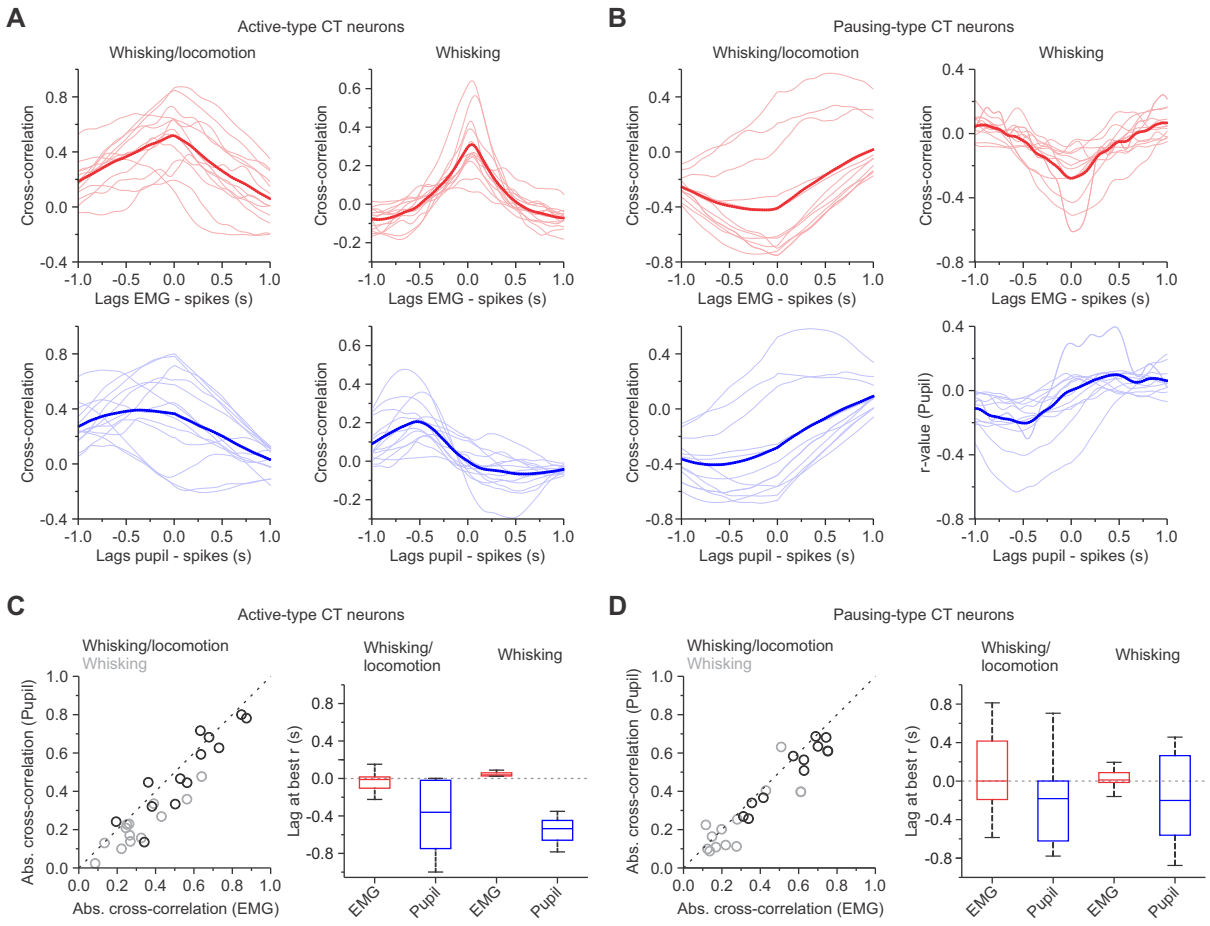
A
Active-type CT neurons
Whisking/locomotion
Whisking
Cross-correlation
Lags EMG - spikes (s)
Lags pupil - spikes (s)
B
Pausing-type CT neurons
r-value (Pupil)
C
Abs. cross-correlation (Pupil)
Abs. cross-correlation (EMG)
Whisking/locomotion
Whisking
Whisking/
locomotion
Lag at best r (s)
EMG
Pupil
D

Figure 5

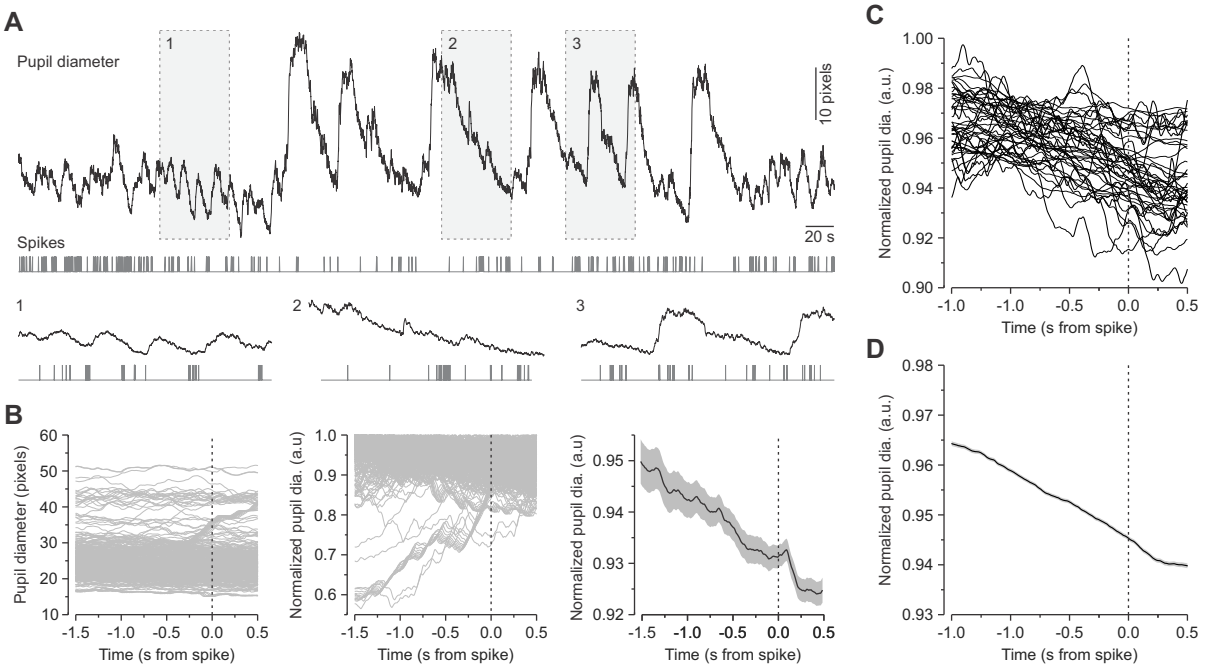
A
Pupil diameter
1
2
3
10 pixels
20 s
Spikes
B
Pupil diameter (pixels)
Normalized pupil dia. (a.u)
Time (s from spike)
C
Normalized pupil dia. (a.u.)
Time (s from spike)
D
Normalized pupil dia. (a.u.)
Time (s from spike)

Figure 6